ロシア・南バイカルKhenteyドーム、Burkal川流域に産するマントル捕獲岩中の単斜輝石の微量元素研究

著者	リタソフ コンスタンチン, 坂本 尚義, リタソフ ユーリ, ラスカゾフ セルゲイ, マルコベッツ ウラジミル, 谷口 宏充, / ユリモト,ヒサヨシ, /, / タニグチ,ヒロミツ, LITASOV Konstantin, YURIMOTO Hisayoshi, LITASOV Yury, RASSKAZOV Sergey, MALKOVETS Vladimir, TANIGUCHI Hiromitsu
journal or publication title	東北アジア研究
number	9
page range	159-178
year	2005-03-28
URL	http://hdl.handle.net/10097/41104

Trace Element Study of Clinopyroxenes from Garnet and Spinel Peridotite Xenoliths of the Burkal River (Khentey dome, South Transbaikalia, Russia)

Konstantin LITASOV[1,2], Hisayoshi YURIMOTO[3], Yury LITASOV[2], Sergey RASSKAZOV[4,5], Vladimir MALKOVETS[6], Hiromitsu TANIGUCHI[5]

Key words : garnet and spinel lherzolite, clinopyroxene, trace elements, upper mantle, metasomatism

Abstract

Trace element chemistry of clinopyroxene in the mantle xenoliths from melanephelinites of the Burkal volcanic group has been studied. The Burkal group is composed of several local outcrops of 5-8 Ma melanephelinites within the Khentey dómal uplift near the Russia/Mongolia boundary. Cr-diopside group xenoliths include garnet and spinel lherzolite, spinel harzburgite and dunite, and garnet and spinel pyroxenites. Hydrous minerals were not detected, however shallow mantle feldspatic metasomatism is present. Clinopyroxene from garnet lherzolites has high TiO_2, Al_2O_3, and Na_2O relative to clinopyroxene from spinel lherzolites. Olivine has composition of Fo_{90-92}. Spinel has Mg#= 60-80 and contains 10-46 wt. % Cr_2O_3. Clinopyroxene from garnet lherzolites has REE patterns typical for fertile peridotites. Trace element patterns of clinopyroxene from depleted spinel peridotites show progressive depletion in HREE and HFSE and enrichment in LREE toward more depleted varieties of harzburgites and dunites. REE patterns of clinopyroxene in harzburgites are strongly U-shaped and have (La/Sm)n=5-36 and (Sm/Yb)n=0.4-2.1. Clinopyroxene in harzburgites has also extremely low Zr content (0.4-3.4 ppm) and high Ti/Zr ratio ranged in 190-240. The patterns of clinopyroxene in depleted

1 Institute of Mineralogy, Petrology and Economic Geology, Faculty of Science, Tohoku University, Sendai, Japan
2 Institute of Geology, SB RAS, Novosibirsk, Russia
3 Department of the Earth's and Planetary Sciences, Tokyo Institute of Technology, Tokyo, Japan
4 Institute of the Earth's Crust, SB RAS, Irkutsk, Russia
5 Center for Northeast Asian Studies, Tohoku University, Sendai, Japan
6 GEMOC National Key Center, Department of Earth and Planetary Sciences, Macquarie University, Sydney, Australia

peridotites are indicative of significant partial melting (up to 15−20%) of the primary substrate followed by cryptic metasomatic enrichment by silicate or carbonatitic melt. Estimation of T-P parameters for garnet lherzolites reveals equilibration at 17-23 kbar (60-90 km depths) and 1050-1150℃. T-estimations for harzburgites and dunites indicate, that they may form veins at 50-70 km depth, whereas shallow mantle (low-T) depleted peridotites were not detected. The uppermost mantle may be composed of fertile spinel lherzolites.

1. Introduction

Many ultramafic and mafic volcanics worldwide contain deep-seated xenoliths, which provide direct information about composition of the upper mantle. In the Baikal rift zone Late Cenozoic basalts containing mantle xenoliths are abundant (Kiselev et al., 1979; Ashchepkov, 1991; Litasov and Taniguchi, 2002). Basaltic volcanic fields may be axial (e.g. Udokan and East Sayan) and off axial (e.g. Vitim and Bartoy) in relation to the central basing of the rift system (Fig. 1). Near axial fields entrained xenoliths of moderately depleted to depleted spinel peridotites with minor or absent signatures of hydrous metasomatism. In contrast off axial fields (corresponding typically to lithosphere slope) entrain xenoliths with fertile mantle or enriched compositions affected by hydrous metasomatic modification (Litasov and Taniguchi, 2002).

Here we report first results on trace element studies of clinopyroxene from Cr-diopside series xenoliths from distinct locality of melanephelinites of the Burkal River situated outside of the rift system within Khentey domal uplift. The xenoliths of Burkal localities were first described by Rasskazov (1987; 1993) and Ashchepkov et al. (1996). Unique position of the locality is determined by thick lithosphere of about 100 km and abundance of garnet-bearing xenoliths allowing to construct a geotherm and describe mantle aside of main rift structures.

2. Geological notes and host volcanics

Formation of Late Cenozoic alkaline basalts in the Baikal rift and adjacent area of Mongolia and development of Baikal Lake and surrounding sedimentary depressions was connected with rifting processes and mantle plume upwelling near south boundary of the Siberian Craton (Logatchev, 1993; Rasskazov, 1994; Delvaux et al, 1997; Litasov and Taniguchi, 2002).

The Burkal group of melanephelinites locates within domal uplift of the Khentey ridge

with lithosphere thickness of about 100 km (this value is thick relative to rift zone, but thin compared to adjacent areas, Fig. 1). The geological structure of the region is a consequence of existence of long-lived subduction zone at the boundary of the Mongol-Okhotsk Ocean during Late Palaeozoic and its final closure in Late Jurassic-Early Cretaceous (e. g. Belichenko et al., 1994).

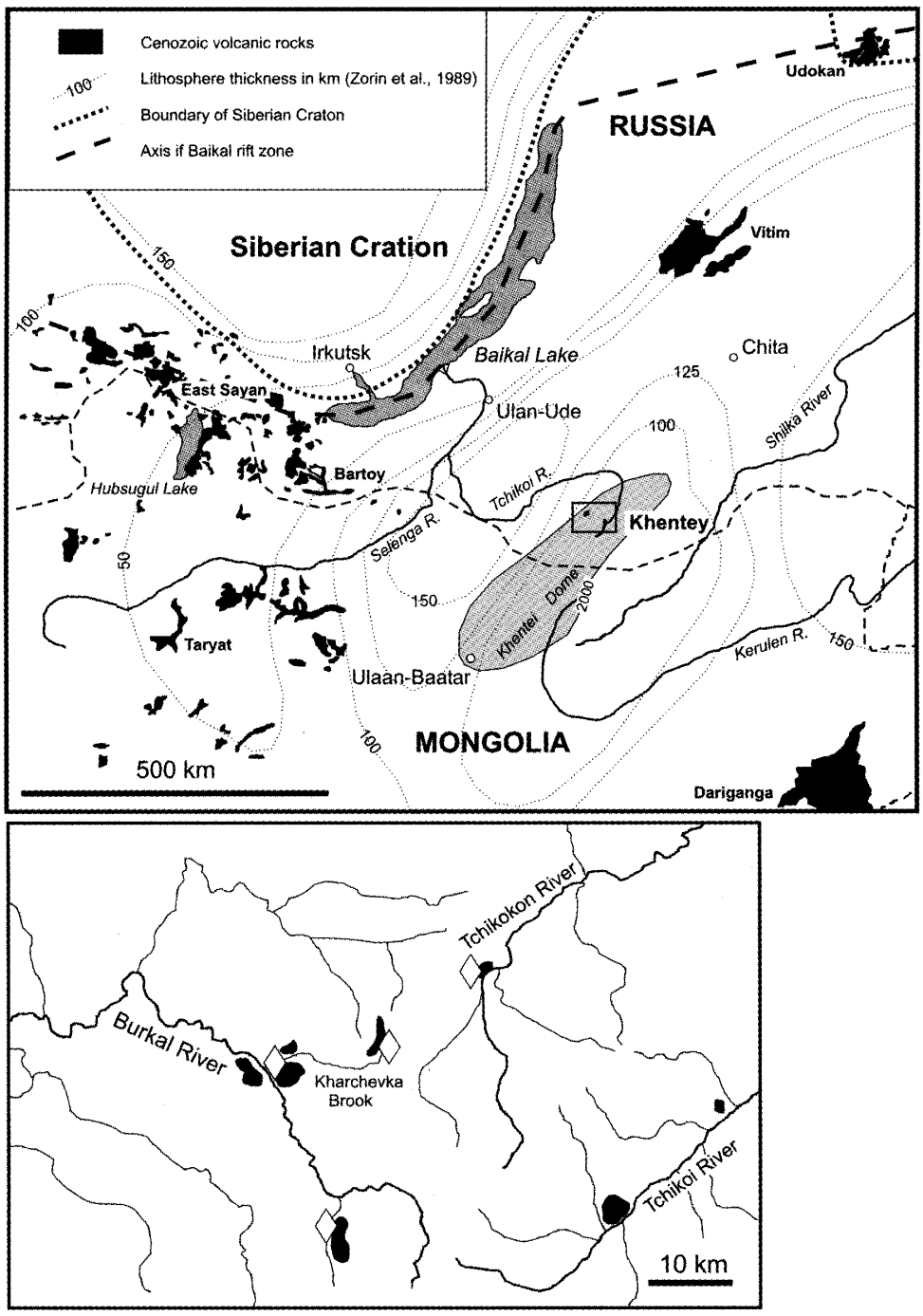

Fig. 1 : (a) Distribution of Cenozoic alkaline basalts and geophysical lithosphere thickness in the Baikal-Mongolia region (after Kiselev et al., 1979 and Zorin et al., 1989). Khentey Dome with altitudes above 2000 m is outlined ; (b) Schematic map of the Burkal locations (after Ashchepkov et al., 1996). *Diamonds*, xenolith occurrences.

Late Cenozoic activity in the region was limited by local melanephelinite eruptions. Melanephelinites are dated by 5.5-8.0 Ma (Polyakov and Bagdasaryan, 1986; Ashchepkov et al., 2003). Volcanism in Burkal area is temporally connected with significant magmatic activity in Vitim, Hamar-Daban and East Sayan volcanic fields. Major element data for Burkal volcanics were reported by Rasskazov (1987) and Litasov and Taniguchi (2002). The melanephelinites have Mg#=67-69;and contain 41-46 wt.% SiO_2, 4-7 wt.% of Na_2O+K_2O. Abundant mantle xenoliths have been found in lava flows near the mouth of Kharchevka Brook (Fig. 1).

3. Analytical methods

Minerals and glasses were analyzed in polished thin sections and mounts for major elements using JEOL Superprob microanalyzer (JXA-8800) in the Institute of Mineralogy, Petrology and Economic Geology of Tohoku University in Sendai, Japan and Camebax Micro microanalyzer in the United Institute of Geology, Geophysics and Mineralogy in Novosibirsk, Russia. Analyses were run with 15-20 keV acceleration voltages, 10-40 nA

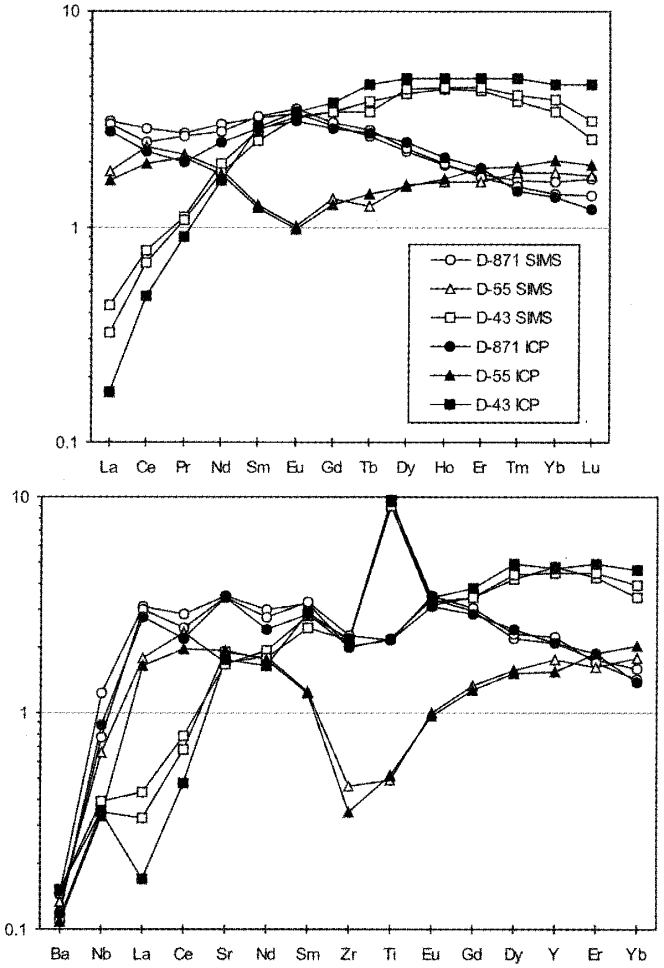

Fig. 2 : Comparison of trace element patterns of standard samples measured by SIMS using calibration by GSJ glasses and by LAM ICP-MS.

sample current, and 1-10 μm beam size. Oxides and natural and synthetic minerals were used as standards. Matrix corrections were performed by the ZAF-procedure.

Secondary ion mass spectrometry measurements were conducted at Tokyo Institute of Technology using Cameca IMS-3F microanalyser. Polished mount with samples were coated with gold film to eliminate electrostatic charge build-up on the surface during analysis. Measurements were made by cycling through mass sequences in a peak jumping mode. Secondary ion signals were detected with en electron multiplier. We used glass standards JB-1a and JR-1 synthesized from GSJ rock reference powders. Detected secondary ion intensities were corrected for natural isotopic abundances and normalized to the intensity of Si (reference mass ^{30}Si). Calibration and corrections of concentrations from the secondary ion intensities have been described elsewhere (Yurimoto et al., 1989). The results were examined by reproducing analyses of clinopyroxene from various spinel lherzolites D-871, D-55 and D-43 of Dzhilinda River (Vitim volcanic field), which were studied earlier by LAM ICP-MS (Litasov and Taniguchi, 2002). The data obtained by SIMS are generally consistent with those by LAM ICP-MS (Fig. 2).

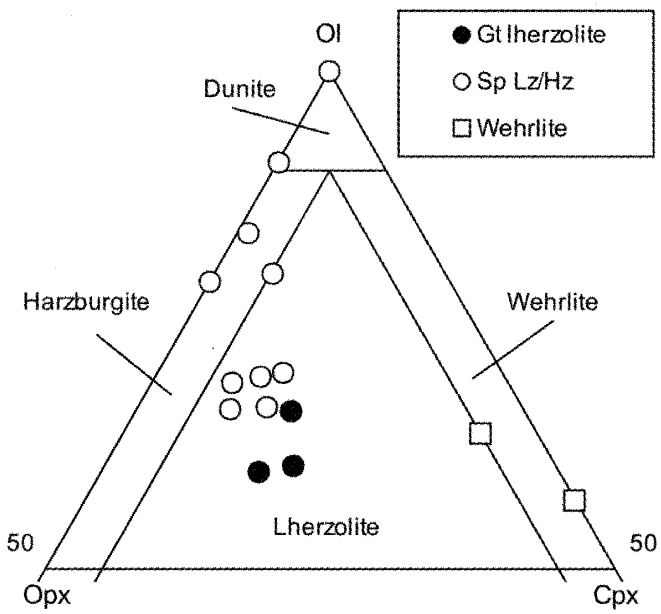

Fig. 3 : Modal composition of Burkal peridotite xenoliths.

4. Mineralogy of xenoliths

Ashchepkov et al. (1996) distinguished several major groups of xenoliths in the Burkal localities: Group I (Cr-diopside) includes garnet and spinel lherzolite, spinel harzburgite and dunite; and garnet and spinel pyroxenites; Group II (Al-augite) includes

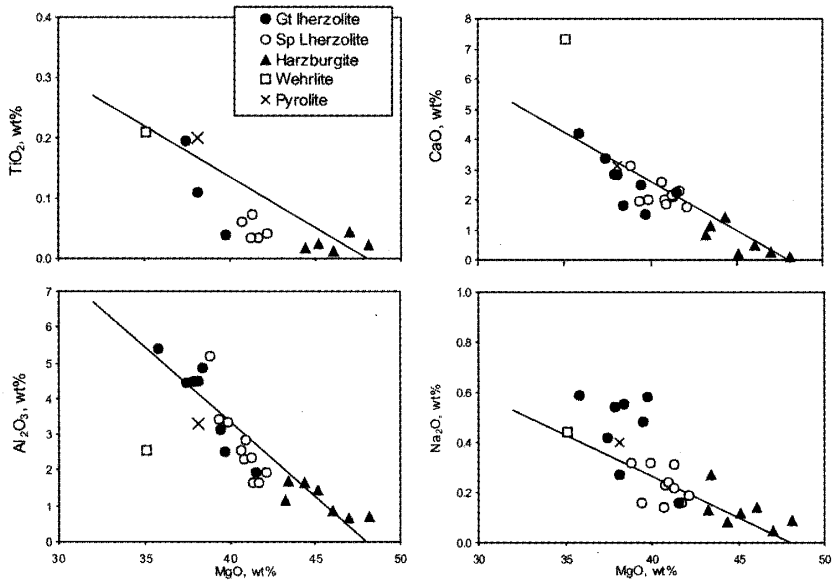

Fig. 4 : Bulk rock composition of the peridotite xenoliths from the Burkal localities. Pyrolite composition is after Ringwood (1977). *Solid lines* indicate linear regression for garnet and spinel lherzolites from picrobasalt, Vitim volcanic field (after Litasov and Taniguchi, 2002)

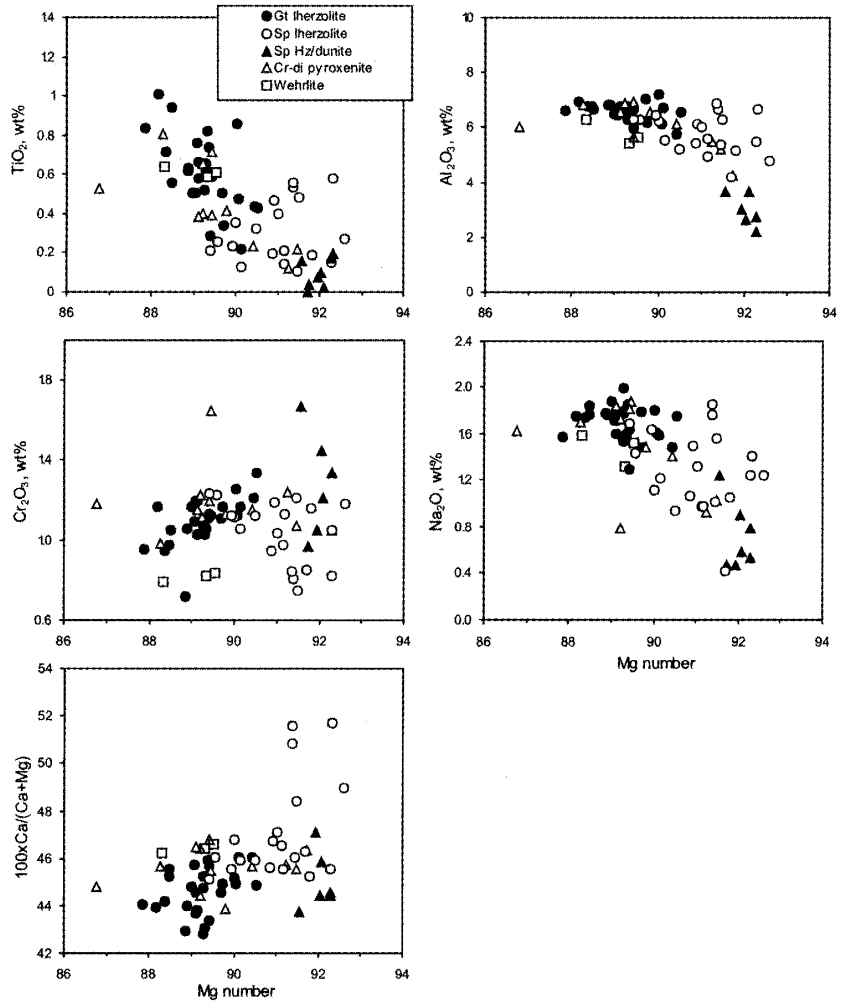

Fig. 5 : Composition of clinopyroxene from Cr-diopside xenoliths of the Burkal localities.

Table 1. Major and trace element composition of clinopyroxene from Cr-diopside series xenoliths in Miocene nephelinites of the Burkal River.

Sample	Bu-6	Bu-15	Bu-2	Bu-4	Bu-16	Bu-57	Bu-95	Bu-25	Bu-59	Bu-10a	Bu-100	Bu-104	Bu-51
Type	Gt lherzolites			Sp lherzolites				Wh	SW	Sp harzburgites			SL
SiO_2	52.77	52.39	51.84	52.22	52.03	52.06	51.70	52.37	52.57	52.95	53.18	52.80	52.07
TiO_2	0.44	0.22	0.86	0.21	0.47	0.58	0.40	0.64	0.13	0.01	0.01	0.03	0.11
Al_2O_3	5.78	6.72	7.20	6.27	6.13	6.69	6.03	6.29	5.39	3.89	4.21	3.67	5.36
Cr_2O_3	1.21	1.17	1.26	1.23	1.19	0.82	1.04	0.79	1.23	1.46	0.85	1.22	1.21
FeO*	3.04	3.03	3.12	3.36	2.80	2.29	2.79	3.73	2.89	2.55	2.83	2.68	2.79
MnO	0.11	0.07	0.04	0.07	0.03	0.07	0.08	0.16	0.08	0.09	0.15	0.07	0.10
MgO	16.13	15.52	15.80	15.94	15.74	14.45	15.84	15.83	16.82	17.89	17.56	17.5	16.76
CaO	19.17	18.42	18.12	18.22	19.18	21.12	19.62	18.95	19.57	20.91	21.06	20.6	19.87
Na_2O	1.48	1.59	1.80	1.70	1.50	1.42	1.32	1.59	1.04	0.41	0.42	0.59	1.01
K_2O	0.02	0.02	0.00	0.00	0.01	0.01	0.03	0.01	0.01	0.01	0.01	0.00	0.01
NiO	0.09	0.08	0.03	0.05	0.02	0.10	0.03	0.02	0.11	0.11	0.09	0.10	0.02
Total	100.2	99.24	100.1	99.28	99.10	99.60	98.87	100.4	99.84	100.3	100.4	99.34	99.29
Mg#	90.4	90.1	90.0	89.4	90.9	91.8	91.0	88.3	91.2	92.6	91.7	92.1	91.5
La	0.78	2.44	1.54	2.46	0.82	0.84	4.88	2.60	4.34	9.75	6.87	5.32	4.02
Ce	2.99	8.40	5.86	8.75	3.00	3.07	12.13	9.29	9.15	10.89	9.48	9.33	7.28
Pr	0.52	1.29	0.96	1.32	0.52	0.54	1.71	1.45	1.04	0.56	0.65	0.89	0.62
Nd	2.93	7.07	5.66	7.22	3.21	3.54	8.70	7.53	4.40	1.45	1.80	2.86	2.34
Sm	1.03	2.08	2.14	2.06	1.26	1.58	2.42	2.38	0.99	0.17	0.23	0.42	0.49
Eu	0.38	0.55	0.66	0.54	0.43	0.60	0.67	0.84	0.26	0.04	0.06	0.09	0.16
Gd	1.39	1.61	2.20	1.73	1.32	2.35	2.00	2.43	0.85	0.12	0.19	0.31	0.50
Tb	0.21	0.25	0.32	0.26	0.22	0.44	0.30	0.37	0.13	0.03	0.04	0.06	0.10
Dy	1.10	1.28	1.70	1.25	1.29	3.14	1.56	1.83	0.72	0.28	0.34	0.39	0.61
Ho	0.18	0.23	0.28	0.21	0.23	0.71	0.23	0.30	0.14	0.08	0.10	0.08	0.12
Er	0.44	0.54	0.59	0.52	0.42	1.89	0.56	0.72	0.35	0.28	0.36	0.24	0.32
Tm	0.06	0.08	0.08	0.07	0.07	0.30	0.08	0.10	0.06	0.06	0.06	0.04	0.04
Yb	0.41	0.53	0.53	0.47	0.56	2.09	0.53	0.67	0.38	0.44	0.46	0.27	0.26
Lu	0.06	0.06	0.07	0.07	0.07	0.34	0.07	0.10	0.04	0.05	0.06	0.03	0.03
Nb	0.32	0.52	0.43	0.57	0.43	0.40	1.38	0.78	1.13	0.67	1.59	0.52	1.18
Sr	60.3	99.5	71.9	101	58.3	57.6	103	147	84.1	55.1	53.1	78.7	59.6
Zr	17.2	14.5	32.5	13.9	17.6	28.2	12.8	69.2	5.00	0.41	0.46	6.89	3.35
Ti	2634	1314	5426	1250	2647	3310	2079	4619	562	93	111	302	738
Y	4.27	5.10	6.09	4.91	5.30	19.2	5.40	7.79	3.50	2.27	2.82	2.05	2.91
Sc	38.1	33.0	34.3	32.9	36.7	63.1	36.2	50.1	41.8	41.3	42.2	43.6	35.6
V	289	246	270	247	273	268	263	293	238	172	181	185	210
Mg# Ol	90.6	90.0	90.3	91.3	90.8	90.6	90.5	89.0		90.8	90.7	90.9	90.7
Mg# Opx	90.8	90.0	89.9	91.6	91.0	91.7	90.9		91.4	91.8	91.3	91.7	91.5
Al_2O_3 Opx	3.8	5.1	5.1	4.5	4.3	4.2	4.7		4.7	3.8	4.3	3.5	4.2
Mg# Sp		75.9	74.5	76.2	75.9	74.5	73.7	74.5	74.0	61.5	73.3	59.5	74.6
Cr# Sp		4.6	19.2	25.7	4.6	28.1	22.6	19.2	26.5	48.0	29.6	59.6	28.0

Major element oxides in wt.%. Trace elements in ppm. The major characteristics of other minerals are shown. Most major element compositions of mineral assemblages are reported by Litasov and Taniguchi (2002). Abbreviations: Ol, olivine; Opx, orthopyroxene; Gt, garnet; Sp, spinel; Wh, wehrlite; SW, spinel websterite; SL, spinel lherzolite. Mg#=100xMg/(Mg+Fe); Cr#=100xCr/(Cr+Al); FeO*=FeO+Fe_2O_3.

spinel websterites. Clinopyroxene, garnet, orthopyroxene, ilmenite, and olivine represent megacryst assemblage. Modal and bulk chemistry as well as petrography and major element chemistry of the xenoliths of the Burkal River were described in detail by Rasskazov (1987, 1993), Ashchepkov et al. (1996) and Litasov and Taniguchi (2002).

Modal compositions of xenoliths are shown in Fig. 3. We should note existence of harzburgite, dunite, and wehrlite xenoliths. Peridotites have Mg#=88-91. The contents of MgO show negative correlation with CaO, Al_2O_3, and TiO_2, (Fig. 4). Garnet lherzolites are rich in Na_2O.

Most of garnet peridotites have protogranular and rarely porphyroclastic microstructure. Garnet is usually rimmed or completely replaced by kelyphitic aggregates. Spinel lherzolite and harzburgite also have protogranular and porphyroclastic microstructures, they sometimes contain dunite veins. Small (2－3 cm) discrete dunite xenoliths were also detected.

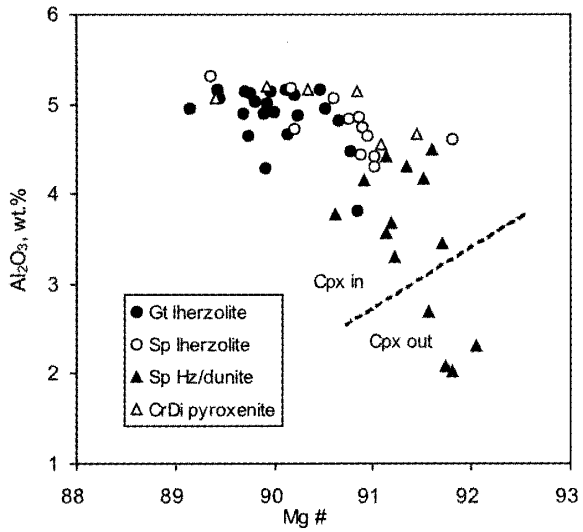

Fig. 6 : Al_2O_3 vs Mg# in orthopyroxene from Cr-diopside xenoliths and megacrysts of the Burkal localities.

Chemistry of the peridotite minerals is generally consistent with modal composition variations from fertile to depleted varieties. Clinopyroxene from garnet lherzolite has high TiO_2, Al_2O_3, and Na_2O relative to those from spinel lherzolite (Fig. 5 ; Table 1). Mg# of clinopyroxene varies from 86 to 93. Some clinopyroxenes from spinel lherzolites have high CaO content and form low-temperature group (see section 6). Orthopyroxene has Mg#=89-92 and contains 4.0-5.4 wt. % Al_2O_3 in garnet and spinel lherzolites (Fig. 6). Orthopyroxene from harzburgites and dunites contains less than 3 wt. % Al_2O_3. Many depleted nodules contain Al-rich orthopyroxene with 3.0-4.5 wt. % Al_2O_3 (Fig. 6). Olivine has composition Fo90-92. Spinel has Mg#=60-80 and contain 10-46 wt. % Cr_2O_3 (Fig. 7). Most peridotites

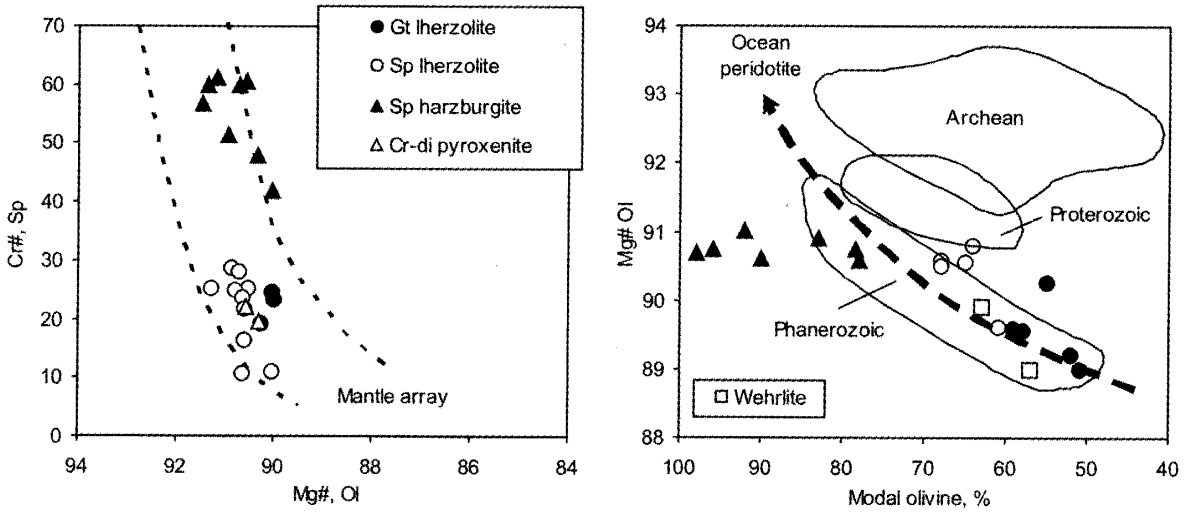

Fig. 7 : (a) Mg# in olivine vs. Cr# in spinel diagram for Burkal xenoliths. Dashed lines indicate boundaries of mantle array (Arai, 1987). Cr#=100Cr/(Cr+Al) ; Mg#=100 Mg/(Mg+Fe). (b) Plot of Mg# in olivine vs modal olivine (%). Oceanic peridotite trend cited from Boyd (1989). Phanerozoic, Proterozoic and Archean areas are from Griffin et al. (1999).

correspond to mantle array in Cr# in spinel versus Mg# in olivine diagram (Fig. 7) and to the field of Phanerozoic lherzolites in the Boyd-Griffin (Boyd, 1989 ; Griffin et al., 1999) diagram (Fig. 7).

Cr-diopside pyroxenites have coarse-equant to protogranular microstructure. Clinopyroxene has lower Mg# than that of lherzolite (Fig. 5). Spinel has low contents of Cr_2O_3 (4-8 wt. %).

Burkal spinel and garnet-spinel lherzolite often contain veinlets with minerals corresponding to the host melanephelinites, but sometimes melt pockets around clinopyroxene and spinel grains are occurred. Some xenoliths contain symplectite-like aggregates between orthopyroxene and olivine grains. These aggregates include clinopyroxene, olivine, and sanidine and were described by Litasov and Taniguchi (2002) and Litasov et al. (2003).

5. Trace element chemistry of clinopyroxenes

Trace element data for clinopyroxenes from the Burkal xenoliths are presented in Table 1 and Fig. 8. Most clinopyroxenes from garnet and spinel lherzolites show REE patterns corresponding to clinopyroxene from primitive garnet lherzolite with slight depletion by LREE and enrichment by HREE with (La/Sm)n=0.4-0.9 (n－normalized to primitive mantle after McDonough and Sun, 1995) and (Sm/Yb)n=2.7-4.4 (Fig. 8a-b). Only one clinopyroxene from spinel lherzolite Bu-57 (low-T group) has pattern analogous to that from typical spinel lherzolite (with high HREE and light depletion by LREE). It has

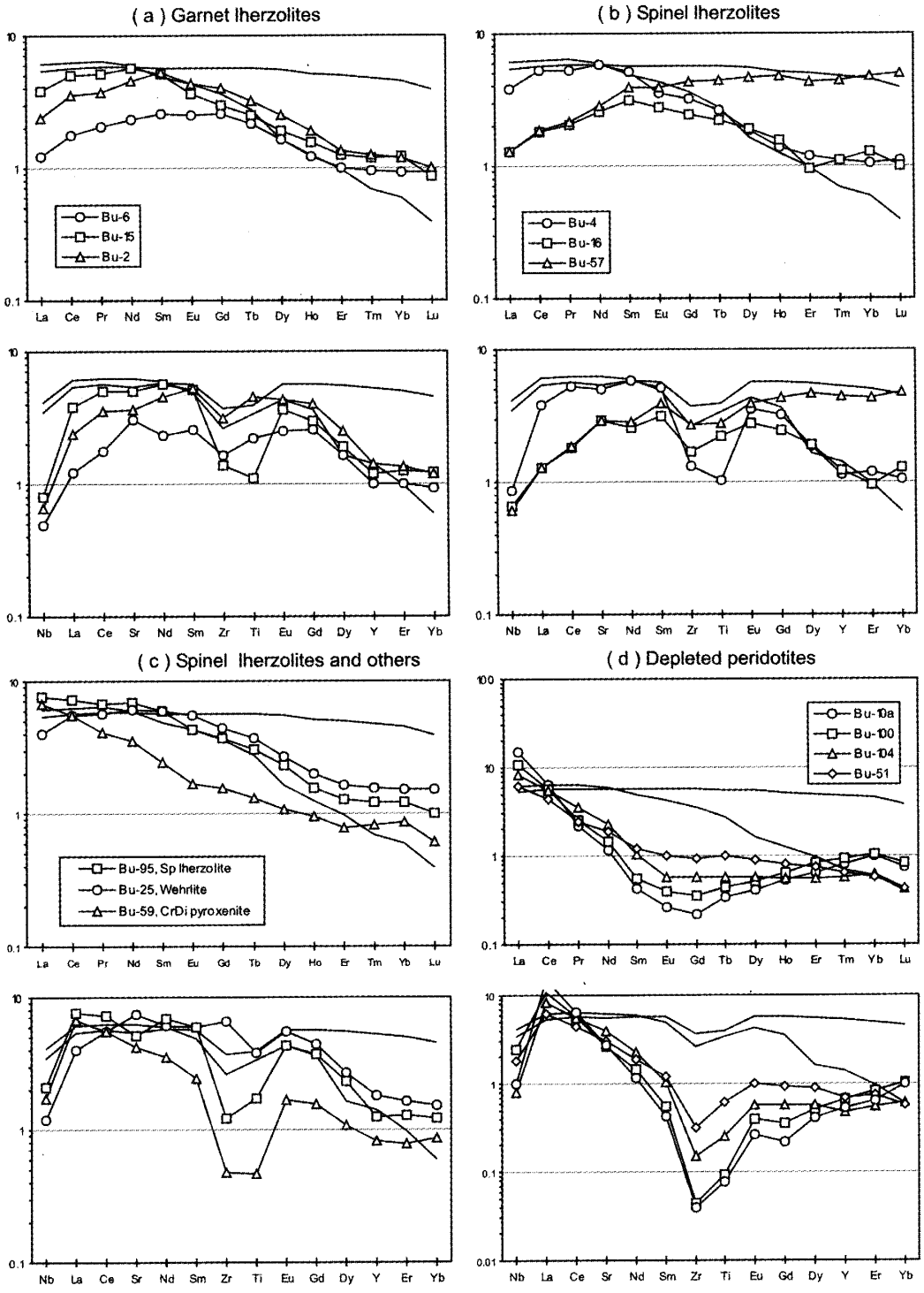

Fig. 8 : Trace element abundances in clinopyroxenes from Burkal xenoliths normalized to primitive mantle of McDonough and Sun (1995).

(La/Sm)n=0.3 and (Sm/Yb)n=0.8. This indicates that many spinel lherzolites were derived from spinel-garnet transition zone, where clinopyroxene is equilibrated with garnet, or undergone significant partial melting and following metasomatism. LREE-enriched clinopyroxenes from Bu-15 and Bu-4 have low Ti/Zr ratios of 89-90 and show positive Sr anomaly (relative to adjacent REE, Ce and Nd), whereas other clinopyroxenes of this series

have Ti/Zr=150-167 and negative Sr anomaly (Fig. 8). Clinopyroxene from wehrlite Bu-25 has almost same REE pattern and low Ti/Zr=66 as that in garnet and spinel lherzolites Bu-4 and Bu-5, but it is significantly enriched in Zr, Ti and Sr (Fig. 8c). Clinopyroxene from pyroxenite Bu-59 is depleted by MREE ((La/Sm)n=2.7 ; (Sm/Yb)n=2.8) and has low concentration of Zr and Ti (Fig. 8c). Clinopyroxene from depleted peridotites has well-defined U-shaped REE patterns with MREE depletion and LEE enrichment with (La/Sm)n=5-36 and (Sm/Yb)n=0.4-2.1 and has significant Zr-Ti negative anomalies (Fig. 8 d), It has high Ti/Zr=190-240 ratio and extremely low Zr concentrations (0.4-3.4 ppm).

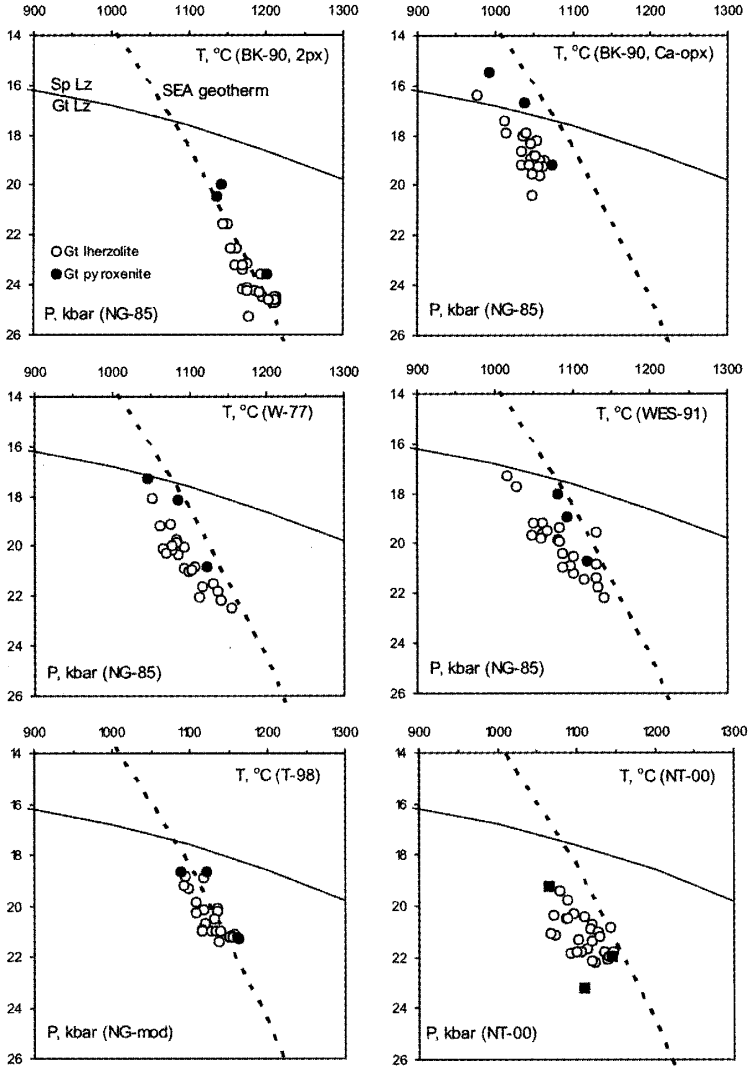

Fig. 9 : P-T-fields for Burkal peridotite and pyroxenite using combinations of the different thermometers and barometers. The southeastern Australia geotherm (SEA : O'Reilly and Griffin, 1985; Xu et al., 1998) is shown for comparison. Solid line is transition boundaries between fertile spinel and garnet lherzolite with Mg#=0.90 and $Cr\#_{Sp}$=0.10 (O'Neill, 1981). BK-90, 2px - two pyroxene thermometer and BK-90, Ca-opx - Ca in orthopyroxene thermometer (Brey and Kohler, 1990); W-77, two-pyroxene thermometer (Wells, 1977); WES-91, Cr-Al in orthopyroxene (Witt-Eickschen and Seck, 1991); T-98, two pyroxene thermometer, (Taylor, 1998); NT-00, enstatite in clinopyroxene thermometer (Nimis and Taylor, 2000). NG-85, Al in orthopyroxene barometer (Nickel and Green, 1985); NG-85, modified NG-85 barometer (Taylor, 1998); NT-00, Cr in clinopyroxene barometer (Nimis and Taylor, 2000).

6. Thermobarometry

Results of T-P calculations for the Burkal xenoliths and list of the thermometers and barometers are shown in Fig. 9-10. We used reference South-Eastern Australia (SEA) geotherm (O'Reilly and Griffin, 1985; Xu et al., 1998) for comparison between different thermobarometers in Fig. 9. Ca-opx, BK-90 and 2-px, BK-90 thermometers combined with NG-85 barometer and N-00 single-clinopyroxene thermobarometer show pure estimations which are inconsistent with garnet-spinel transition boundary or provide scarce results. The results by W-77, WES-91, and TA-98 combined with NG-85 barometer show good estimations and correspond to the geotherm which is consistent or slightly colder than reference SEA geotherm (Fig. 9). T-histograms (Fig. 10) show that temperatures of depleted peridotites (950-1150℃) are only slightly lower than those of garnet lherzolites (1000-1200 ℃), whereas spinel lherzolites with lower temperatures (800-900℃) are also abundant. Temperature distribution for spinel lherzolites is bimodal in most histograms.

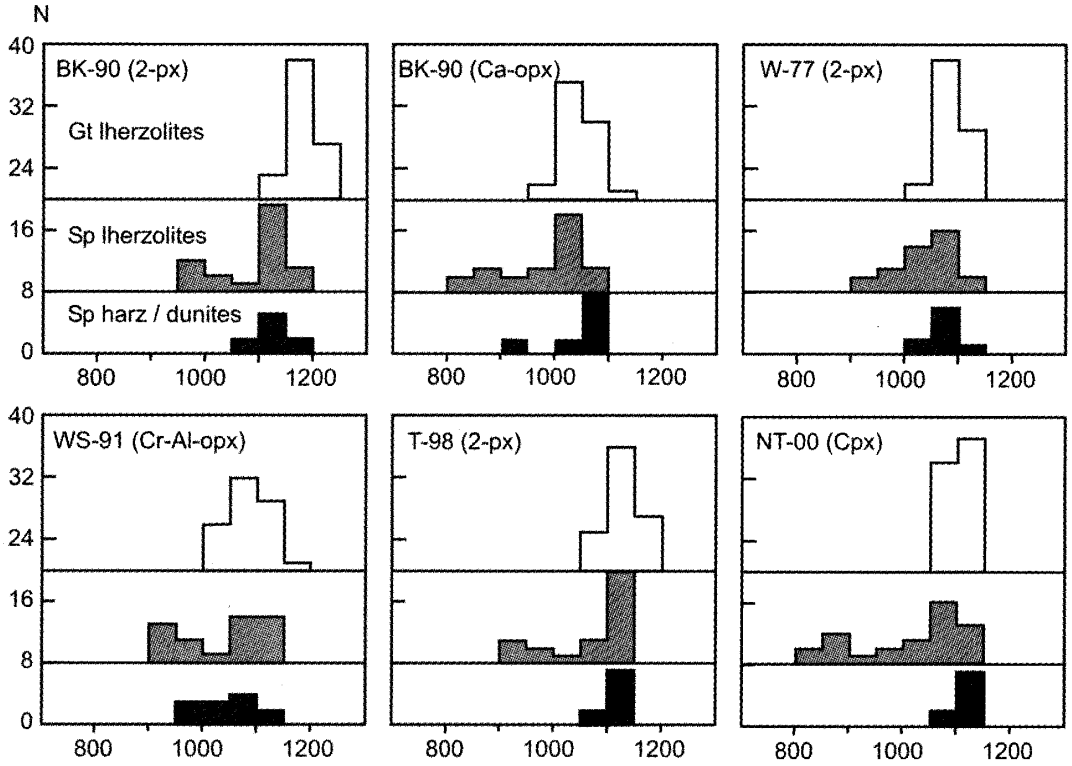

Fig. 10 : Temperature histograms for Burkal peridotites using different thermometers (see Fig. 9 for abbreviations). N, number of samples.

7. Discussion

7.1. Mantle section beneath Khentey dome

Mantle xenoliths from the Burkal River melanephelinite represent mantle domain aside of the Rift system, which locates within domal uplift of the Khentey mountains. It is separated from the rift structures underlain by thin 50 km lithosphere by block with

thick (>150 km) lithosphere under Mesozoic Mongol-Stanovoy zone of the metamorphic core complexes (e. g. Belichenko et al., 1994). Abundant dunite xenoliths and dunite veins in lherzolite suggest strong depletion of the mantle (Litasov and Taniguchi, 2002). Hydrous metasomatic modification was not detected, however shallow mantle feldspatic metasomatism similar with that in the Hamar-Daban (Ionov et al., 1995) and Udokan (Litasov and Taniguchi, 2002 ; Litasov et al., 2003) was observed. Pyroxenite xenoliths of the both Cr-diopside and Al-augite series are rare.

Estimation of T-P parameters for garnet lherzolites reveals equilibration at 17-23 kbar (60-90 km depths) and 1050-1150℃. The constructed geotherm almost coincides with hottest geotherms of South Baikal regions (Bartoy and East Sayan, see Fig. 69 in Litasov and Taniguchi, 2002). High T-estimations for harzburgites and dunites indicate that they may form abundant veins and lenses at 50-70 km depth, whereas shallow mantle (low-T) depleted peridotites were not detected. Uppermost mantle may be composed of fertile spinel lherzolites. This fact is unusual for Baikal region, because in the most other areas, in particular in axial fields (East Sayan, Hamar-Daban, Udokan), depleted peridotites compose the uppermost mantle level. It might be connected with the voluminous volcanic eruptions (relative to Burkal area) and thin lithosphere of axial volcanic fields, where melting could possess uppermost mantle levels.

Although depleted harzburgite and dunite xenoliths are abundant within the Burkal suite most peridotites contain olivine with relatively low Mg# and plot within 'oceanic trend' of Boyd (1997; Fig. 7). No sample falls within the field of Archean peridotites; this strongly implies that no Archean lithosphere has been sampled from Burkal. Most spinel and garnet lherzolites plot along 'oceanic trend' and may represent oceanic peridotite thrust of Mongol-Okhotsk Ocean under the continental margins. It is most likely that garnet lherzolites represent little modified asthenospheric mantle, which have been emplaced beneath the continent to grow the continental lithosphere after closure of the Mongol-Okhotsk Ocean.

7. 2. Depletion and melt percolation signatures

Recent studies showed that majority of the depleted harzburgite and dunite xenoliths in alkaline basalts are not only fragments of refractory residues after partial melting of primitive mantle, but also the products of percolation of small fraction metasomatic melts through peridotite (e. g. Bodinier et al., 1990; Van der Wal and Bodinier, 1996). According to these models of chromatographic percolation, small melt fraction first affects LREE in clinopyroxene and in the final stage clinopyroxene became enriched in the both the LREE

and MREE, thus reflecting the composition of unmodified metasomatizing melt (Navon and Stolper, 1987). Different melt/rock reactions may cause also HFSE (like Nb, Ta, Zr, Hf, Ti, V) depletion and Sr-enrichment (in case of carbonatite melt) (e. g. Bedini et al., 1997; Ionov et al., 2002).

Modelling of partial melting indicates that clinopyroxenes in depleted peridotites of the Burkal River correspond to 10-20% of fractional melting of primitive mantle as it is seen in Ti-Zr, Sm-Zr and Y-Yb plots (Fig. 11). However, we can not model Zr-Ti using typical mineral/basaltic melt partition coefficients (Ds). We can distinguish at least three reasons for this anomalous behavior of Ti, discussed in many papers: (1) carbonatitic melt metasomatism (Hauri et al., 1993; Ionov, 1998; Mal'kovets et al., 1998); (2) basaltic melt metasomatism and fractionation of minor phases, like rutile (Bodinier et al., 1996; Bedini et al., 1997); (3) changes of Ti partition coefficient between peridotite minerals and melt in dependence of melt composition and melting conditions (Vannucci et al., 1998; Xu et al., 2000).

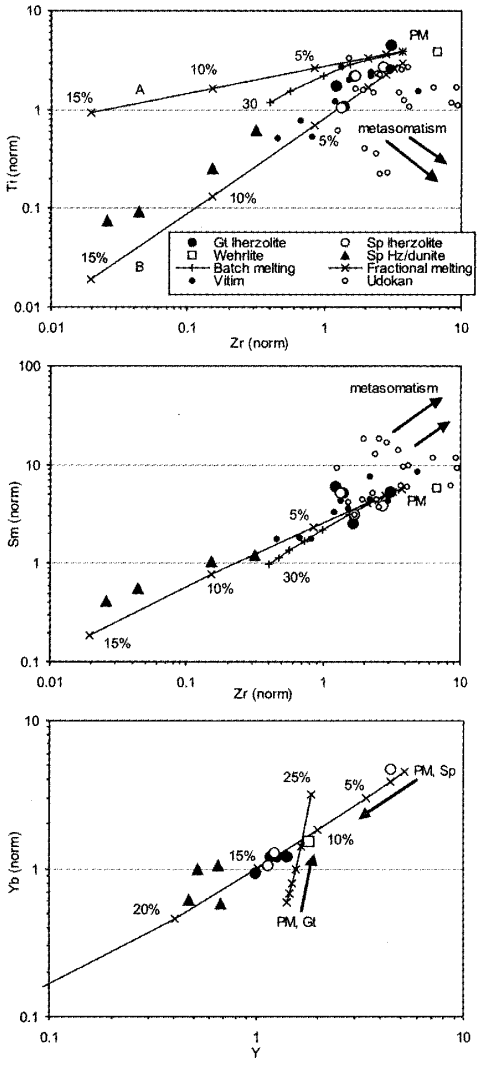

Fig. 11 : Fractional and batch melting models of Ti and Zr, Sm and Zr, and Y and Yb normalized to primitive mantle after McDonough and Sun (1995) and plots of clinopyroxenes from peridotites of Burkal and other Late Cenozoic basaltoids of Transbaikal region (Vitim and Udokan, after Litasov and Taniguchi, 2002). PM, primitive mantle composition (starting point for melting models); PM, Sp and PM, Gt are clinopyroxene from primitive spinel and garnet lherzolites, respectively. Degrees of partial melting are shown in percentages. Set of partition coefficients (D) are reported by Litasov et al. (2000). In Ti-Zr plot line A is calculated using normal partition coefficients and line B is calculated using $D_{Ti}Cpx=0.1$ and D_{Ti} for other minerals lower in factor of 2 than normal Ds.

Significant LREE enrichment of clinopyroxene in harzburgite xenoliths (Fig. 8) indicates that they were affected by a metasomatic melt. As well, Ti-anomalies may be also explained by influence of this melt and D_{Ti}cpx / melt might be very low (ca. 0.1-0.15, Fig. 11). In present work we can not distinguish the nature of metasomatising melt. Some Sr-enrichment of the clinopyroxenes and existence of wehrlite xenoliths (e.g. Yaxley et al., 1998) indicate influence of carbonatite melt, whereas we can not estimate other important characteristics, like Zr/Hf-ratios and carbonatite signs from whole rock trace element chemistry.

8. Conclusions

1. Trace element chemistry of clinopyroxene in Cr-diopside group xenoliths from 5-8 Ma melanephelinites of the Burkal volcanic group located within the Khentey domal uplift near the Russia/Mongolia boundary has been studied. The xenoliths include garnet and spinel lherzolite, spinel harzburgite and dunite, and garnet and spinel pyroxenites. Clinopyroxene from garnet lherzolites has REE patterns typical for fertile peridotites. Trace element patterns of clinopyroxene from depleted spinel peridotites show progressive depletion in HREE and HFSE and enrichment in LREE toward more depleted varieties of harzburgites and dunites.

2. REE patterns of clinopyroxene in harzburgites are strongly U-shaped and have (La/Sm)n=5.36 and (Sm/Yb)n=0.4-2.1. Clinopyroxene in harzburgites has also extremely low Zr content (0.4-3.4 ppm) and high Ti/Zr ratio ranged in 190-240. The patterns of clinopyroxene in depleted peridotites are indicative for significant partial melting (up to 15-20%) of primary substrate followed by cryptic metasomatic enrichment by silicate or carbonatitic melt.

3. Estimation of T-P parameters for garnet lherzolites reveals equilibration at 17-23 kbar (60-90 km depths) and 1050-1150℃. T-estimations for harzburgites and dunites insicate they may form veins at 50-70 km depth, whereas shallow mantle (low-T) depleted peridotites were not detected. Uppermost mantle may be composed of fertile spinel lherzolites.

Acknowledgements

We thank to Y. Ito for help in EPMA. KL acknowledges a Center for Northeast Asian Studies (CNEAS), Tohoku University and Japanese Society for Promotion of Sciences for Research Fellowships during 1999-2004.

References

Arai, S., 1987

An estimation of the least depleted spinel peridotite on the basis of olivine-spinel mantle array. *Neues Jahrbush Mineral. Mh.*, 8, 347-354.

Ashchepkov, I. V., 1991

Deep-seated xenoliths of the Baikal rift, Nauka, Novosibirsk (in Russian).

Ashchepkov, I. V., Litasov, Y. D., and Litasov, K. D., 1996

Garnet peridotite Xenoliths from melanephelinites of Kheney range (South Baikal), *Russ. Geol. Geophys.*, 37 (1), 130-147.

Ashchepkov, I. V., Travin, A. V., Saprykin, A. I., Andre, L., Gerasimov, P. A., and Khmelnikova, O. S., 2003

Age of xenolith-bearing basalts and mantle evolution in the Baikal rift zone, *Russ. Geol. Geophys.*, 44 (11), 1160-1188.

Bedini, R. M., Bodinier, J.-L., Dautria, J.-M. and Morten L., 1997

Evolution of LILE-enriched small melt fractions in the lithospheric mantle: a case study from the East African rift, *Earth Planet. Sci. Lett.*, 153, 67-83.

Belichenko, V. G., Sklyarov, E. V., Dobretsov, N. L., and Tomurtogoo, O., 1994

Geodynamic map of the Paleo-Asian ocean (eastern part), *Russ. Geol. Geophys.*, 35 (7-8), 29-40.

Bodinier, J. L., Vasseur, G., Vernieres, J., Dupuy, C. and Fabries J., 1990

Mechanism of mantle metasomatism: geochemical evidence from the Lherz orogenic peridotite, *Jour. Petrol.*, 31, 597-628.

Bodinier, J. L., Merlet, C., Bedini, R. M., Simien, F., Remaldi, M. and Garrido, C. J., 1996

Distribution of niobium, tantalum and other highly incompatible trace elements in the lithospheric mantle: the spinel paradox, *Geochim. Cosmochim. Acta*, 60, 545-550.

Boyd, F. R., 1989

Composition and distinction between oceanic and cratonic lithosphere, *Earth planet. Sci. Lett.*, 96, 15-26.

Brey, G. P. and Kohler, T., 1990

Geothermobarometry in four-phase lherzolites II. New thermobarometers, and practical assessment of existing thermobarometers, *Jour. Petrol.*, 31, 1313-1336.

Delvaux, D. Moeys, R., Stapel, G., Petit, C., Levi, K., Miroshnichenko, A., Ruzhich, V., and San'kov, V., 1997

Paleostress reconstructions and geodynamics of the Baikal region, Central Asia, Part II. Cenozoic rifting, *Tectonophys.*, 282, 1-38.

Griffin, W.L., O'Reilly, S.Y., and Ryan, 1999

The composition and origin of sub-continental lithospheric mantle, In Fei, Y., Bertka, C.M., and Mysen, B.O. eds., *Mantle petrology: Field observations and high-pressure experimentation: A tribute to Francis R. (Joe) Boyd.* The Geochem. Soc., Spec. publ., 6. Dept. Chem. Univ. Houston, Houston, TX, pp. 13-45.

Hauri, E.H., Shimizu, N., Dieu, J.J., and Hart, S.R., 1993

Evidence for hotspot-related carbonatite metasomatism in the oceanic upper mantle, *Nature*, 365, 221-227.

Ionov, D.A., O'Reilly, S.Y., and Ashchepkov, I.V., 1995

Feldspar-bearing lherzolite xenolith in alkali basalts from Hamar-Daban, southern Baikal region, Russia, *Contrib. Mineral. Petrol.*, 118, 131-148.

Ionov, D.A., 1998

Trace element composition of mantle-derived carbonates and coexisting phases in peridotite xenoliths from alkali basalts, *Jour. Petrol.* 39, 1931-1941.

Ionov, D.A., Bodinier, J.L., Mukasa, S.B., Zanetti, A., 2002

Mechanism and sources of mantle metasomatism: major and trace element compositions of peridotite xenoliths from Spitsbergen in the context of numerical modelling, Jour. Petrol., 43, 2219-2259.

Kiselev, A.I. and Medvedev, M.E., and Golovko, G.A., 1979

Volcanism of the Baikal rift zone and problems of deep magma generation, Nauka, Novosibirsk (in Russian).

Litasov, K.D., Litasov, Y.D., Mekhonoshin, A.S., and Mal'kovets, V.G., 2000

Geochemistry of clinopyroxenes and petrogenesis of mantle xenoliths from Pliocene basanites of the Dzhilinda River (Vitim volcanic field), *Russ. Geol. Geophys.*, 41, 1555-1572.

Litasov K.D. and Taniguchi H., 2002

Mantle evolution beneath Baikal rift, Center for Northeast Asian Studies, Tohoku University, Japan, CNEAS Monograph Series, v. 5.

Litasov, K.D., Sharygin, V.V., Simonov, V.A., Mal'kovets, V.G., and Taniguchi, H., 2003

Petrogenesis of glasses and microphenocrysts in mantle xenoliths from Baikal-Mongolia region: a review, *Northeast Asian Studies*, 8, 127-170.

Logatchev, N. A., 1993

History and geodynamics of the Baikal rift (east Siberia) : a review, *Bull. Centr. Rech. Expl or. Prod. Elf Aquitaine*, 17 (2), 353-370.

Mal'kovets, V. G., Ionov, D. A., Griffin, W. L., O'Reilly, S. Y., Pokhilenko, N. P., and Litasov, K. D., 1998

A P-T-composition cross-section of spinel and garnet facies lithospheric mantle in the Minusa region SW of the Siberian craton. Ext. Abst. 7th Int. Kimb. Conf., Cape Town, South Africa, pp. 543-545.

McDonough, W. F. and Sun, S. S., 1995

The composition of the Earth, *Chem. Geol.*, 120, 223-253.

Navon, O. and Stolper, E., 1987

Geochemical concequences of melt percolation: The upper mantle as a chromatographic column, *Jour. Geol.*, 95, 285-307.

Nickel, K. G. and Green, D. H., 1985

Empirical geothermobarometry for garnet peridotites and implications for the nature of the lithosphere, kimberlites and diamonds, *Earth Planet. Sci. Lett.*, 73, 158-170.

Nimis, P. and Taylor, W. R., 2000

Single clinopyroxene thermobarometry for garnet peridotites. Part I. Calibration and testing of a Cr-in-Cpx barometer and an enstatite-in-Cpx thermometer, *Contrib. Mineral. Petrol.*, 139, 541-554.

O'Neill, H. St. C., 1981

The transition between spinel lherzolite and garnet lherzolite, and its use as geobarometer, *Contrib. Mineral. Petrol.*, 77, 185-194.

O'Reilly, S. Y. and Griffin, W. L., 1985

A xenolith-derived geotherm for Southeastern Australia and its geophysical implications, *Tectonophys.*, 111, 41-63.

Polyakov, A. I. and Bagdasaryan, G. P., 1986

The age of the young volcanoes of the East Siberia and regular compositional evolution of volcanics, *Geochem. Int.*, 3, 311-317.

Rasskazov, S. V., 1987

Deep-seated inclusions in Late Cenozoic melanephelinites from the South of the Central Transbaikalia, *Russ. Geol. Geophys.*, 28 (7), 50-60.

Rasskazov, S. V., 1993

Magmatism of Baikal rift system. Nauka, Novosibirsk (in Russian).

Rasskazov, S. V., 1994

Magmatism related to the Eastern Siberia rift system and the geodynamics, *Bull. Centres Rech. Explor.-Prod. Elf Aquitaine*, 18 (2), 437-452.

Ringwood, A. E., 1977

Basaltic magmatism and the bulk composition of the Moon. I. Major and heat-producting elements, *The Moon*, 16, 389-423.

Taylor, W. R., 1998

An experimentl test of some geothermometer and geobarometer formulations for upper mantle peridotites with application to the thermobarometry of fertile lherzolite and garnet websterite, *Neues Jahrbush Mineral. Abh.*, 172, 381-408.

Van der Wal, D. and Bodinier, J.-L., 1996

Origin of the recrystallization front in the Ronda peridotite by km-scale pervasive porous melt flow, *Contrib. Mineral. Petrol.*, 122, 387-405.

Vannucci, R., Bottazzi, P., Wulff-Pedersen, E., and Newmann, E.-R., 1998

Partitioning of REE, Y, Sr, Zr and Ti between clinopyroxene and silicate melts in the mantle under La Palma (Canary Islands) : implications for the nature of the metasomatic agents, *Earth Planet. Sci. Lett.*, 158, 39-51.

Wells, P. R. A., 1977

Pyroxene thermometry in simple and complex systems, *Contr. Miner. Petrol.*, 62, 129-139.

Witt-Eickschen, G. and Seck, H. A., 1991

Solubility of Ca and Al in orthopyroxene from spinel peridotite: an improved version of an empirical geobarometer, *Contrib. Mineral. Petrol.*, 106, 431-439.

Xu, X., O'Reilly, S. Y., Griffin, W. L., Zhou, X., and Huang, X., 1998

The nature of the lithosphere at Nushan, Eastern China, *In* Flower, M. F. J. ed. *Mantle dynamics and plate interactions in East Asia*, AGU, Washington, Geodyn. series, 27, pp. 167-195.

Xu, X., O'Reilly, S. Y., Griffin, W. L., and Zhou, X., 2000

Genesis of young lithospheric mantle in Southeastern China: an LAM-ICPMS trace element study, *Jour. Petrol.*, 41, 111-148.

Yaxley, G. M. and Green, D. H. 1998

Reactions between eclogite and peridotite: mantle refertilisation by subduction of oceanic crust, *Schweiz. Min. Petr. Mitt.* 78, 243-255.

Yurimoto, H., Yamashita, A., Nishida, N., and Sueno, S., 1989
Quantitative SIMS analysis of GSJ rock reference samples, *Geochem. Jour.*, 23, 213-236.

Zorin, Y. A., Kozhevnikov, V. M., Novoselova, M. R., and Turutanov, E. H., 1989
Thickness of the lithosphere beneath the Baikal rift zone and adjacent regions, *Tectonophys.*, 168, 327-337.